Water Reflection Recognition via Minimizing Reflection Cost Based on Motion Blur Invariant Moments

Sheng-hua Zhong [1], Yan Liu [1], Ling Shao [2], Fu-lai Chung [1]

[1] Department of Computing, The Hong Kong Polytechnic University, Hong Kong, P. R. China

[2] Department of Electronic and Electrical Engineering, University of Sheffield, Sheffield, United Kingdom

{csshzhong@comp.polyu.edu.hk, csyliu@comp.polyu.edu.hk, ling.shao@sheffield.ac.uk, cskchung@comp.polyu.edu.hk }

ABSTRACT

Water reflection, a kind of typical imperfect reflection symmetry problem, plays an important role in image content analysis. However, existing techniques of symmetry recognition cannot recognize water reflection images correctly because of the complex and various distortions caused by water wave. To address this difficulty, we construct a novel feature space which is composed of motion blur invariant moments. Moreover, we propose an efficient detection algorithm to determine the reflection axis in images with water reflection. By experimenting on real image dataset with different tasks, the proposed techniques demonstrate impressive results in the water reflection image classification, the reflection axis detection, and the retrieval of the images with water reflection.

Categories and Subject Descriptors

I.4.9 [**Computing Methodologies**]: Dynamic Programming Based on Motion Blur invariant Moment -*Applications*

General Terms

Algorithms, Performance, Experimentation.

Keywords

Water reflection, imperfect symmetry, motion blur, moment invariants, reflection axis detection.

1. INTRODUCTION

Reflection is the change in direction of a wavefront at an interface between two different media so that the wavefront returns into the medium from which it originated. As one kind of reflection, water reflection happened between the scenery and water attracts many artists and photographers. In natural image analysis, water reflection plays an important role. First, water reflection itself is an exciting natural landscape, so images with water reflection should be considered as one important category of natural images. Experiments from psychology reveal that subjects give favorable ratings to the scene with reflective water [1]. Second, whether being

aware of the existing of water reflection will greatly influence the further image analysis, such as image segmentation and object recognition. Figure 1(a) is an image with water reflection, and the correct segmentation result is shown in Figure 1 (b). However, most existing segmentation algorithms, for example, graph-based technique presented in [2], will partition the mountain and its reflection as one segment as shown in Figure 1 (c), if the existing of water reflection is not known previously. More importantly, it is difficult to recognize the object mountain according to the wrong segmentation. Obviously, the shape and the location information in Figure 1 (c) will be helpless to detect the mountain. Figure 1 (d) is the color histogram of the mountain part in Figure 1(a). Figure 1 (e) shows the color histogram of the mountain and the reflection. It is obvious that partitioning the object and the reflection as one part will distort the color feature for recognition.

(a)
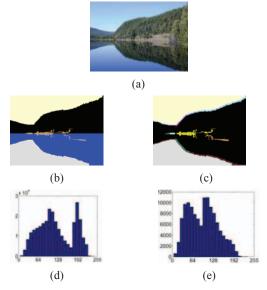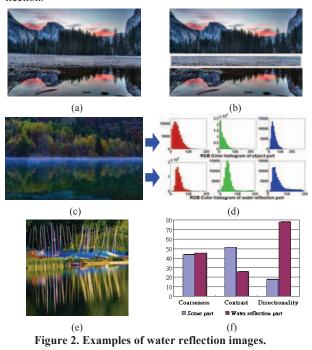

(b)   (c)

(d)   (e)

Figure 1. Example of the influence from water reflection to image segmentation and object recognition. (a) is an example image with water reflection. (b) is the correct segmentation result. (c) is the actual segmentation using existing algorithms. (d) is the color histogram of the mountain. (e) is the color histogram of the mountain and the reflection.

Although water reflection has been known as an exciting and favorable nature landscape, to our knowledge, no existing technique has been proposed to address water reflection image classification and only one paper [3] proposed to detect water reflection axis. But the flip invariant shape detector utilized in [3] relies on the

sharp of water reflection part is complete and distinct. Actually, the water reflection is a complex and various phenomena leading to the modeling and recognition difficulty. As shown in Figure 2 (a) and (b), the snow mountain and trees are partially reflected because the ice covers some area of the lake. Figure 2 (c) and Figure 2 (d) demonstrate the color distortion of the forest after reflection. Obviously, the red information loses a lot. In Figure 2(f), three most important Tamura texture features from the scene part and water part are compared. There exist great differences of contrast and directionality between the original object and its reflection.

(a)   (b)

(c)   (d)

(e)   (f)

Figure 2. Examples of water reflection images.

This paper formulates the water reflection recognition as an imperfect reflection symmetry problem, which has been studied for more than twenty years in computer vision. To address the special characteristics of water wave, we construct a novel feature space which is invariant to motion blur caused by the relative motion of the water part in finite exposure time of human's eyes or other kinds of sensors. Moreover, we design an efficient detection algorithm to recognize the images with water reflection and to detect the reflection axis as well.

The rest paper is organized as follows. Section 2 reviews previous work about symmetry, especially imperfect reflection symmetry. In section 3, we discuss the limitations of using existing feature space in water reflection detection task and propose a motion blur invariance space (MBIS) according to the characteristics of water wave. Section 4 formulates the water reflection recognition to the optimization problem and provides an efficient solution using dynamic programming (DP). Experiments on real dataset are reported in section 5. The paper is closed with conclusion.

2. PREVIOUS WORK

Symmetry is an essential and ubiquitous concept in nature, science, and art. The problem of symmetry detection has been extensively studied in numerous fields including visual perception, computer vision, and computational geometry. The goal of the research on symmetry roughly includes recognition of the symmetry group [4], determination of the axis of symmetry or affinely [5] [6] and perspectively distorted symmetry detections [7] [8].

Reflection symmetry is a type of symmetry in which one half of the object is indistinguishable from its mirror transformed image of the other as shown in Figure 3 (a). As one of the most common basic symmetries [9], reflection symmetry has been used in many different fields for various applications from face analysis [10], vehicle detection [11] to medical image analysis [12]. Since the restriction to exact symmetries limits the use of these methods for real-world objects, more and more work focused on the imperfect symmetry as shown in Figure 3 (b). Two types of imperfect symmetry are studied. Local symmetry means a portion of a model is perfectly symmetric while the rest of it is not. Approximate symmetry means the entire model is not symmetric but could be made symmetric with a slight deformation [13].

(a)   (b)

Figure 3. Examples of symmetry images. (a) is perfect symmetry, (b) is curved glide-reflection imperfect symmetry.

Based on the nature of the features extracted from images, the existing algorithms for reflection symmetry detection can be roughly classified into two general approaches, namely, global versus local approaches [14]. In global approaches, some of algorithms are based on the global features, especially in Fourier domain. For example, Lucchese [15] proposed an elegant approach to analyze the angular properties of an image in Fourier domain. And Derrode et al. [16] analyzed the symmetries of real objects by computing the Analytic Fourier-Mellin transform (AFMT). Different from researches in Fourier domain, [17] considered the entire contour at once when finding the axes of skewed symmetries. Because the use of local features is one of the corner stones of modern computer vision, recent work emphasizes the use of local image features. The representative one is scale-invariant feature transform (SIFT) descriptor. Loy *et al.* [18] chose detection points as interesting salient points and took advantage of pairwise matching of their SIFT descriptors to detect the axis of symmetry. Some other existing work focused on the shape characteristic of symmetry. For example, local invariants computed as single points [19] [20] on the curves or statistically compare pairs of contour points [21] [22].

3. FEATURE SPACE IN WATER REFLECTION RECOGNITION

In this section, we discuss the limitations of using existing feature space of symmetry detection in water reflection problem. Then we analyze the feature space distortion caused by motion blur. Third, we construct a novel feature space called motion blur invariance space (MBIS).

3.1 Limitation of Existing Feature Space for Water Reflection Recognition

For global approach of reflection symmetry detection, features from Fourier domain are always used. In [15], Lucchese proved that if an image $\psi(x), x \in \mathbb{R}^2$ having reflection symmetry with

respect to the reflection axis $y = x \times \tan\alpha$, their Fourier transform $\psi(k), k \in \mathbb{R}^2$, has the same reflection symmetry with respect to the line $k_y = k_x \times \tan\alpha$. The difference between the original one and the reflection one will be much smaller than the difference of other parts. But due to the characteristics of water part, this conclusion is not always true. Figure 4(a) is an image with water reflection. Figure 4(b) is the image with the real reflection axis. We calculate the Fourier transform with this real reflection axis. Based on Figure 4(d) which is the Fourier transform $\psi(k)$ results of object part and water part, we find the $\psi(k)$ do not have reflection symmetry as expected. The average difference of object part and water reflection part is much larger than fake symmetry axis marked just as in Figure 4(c).
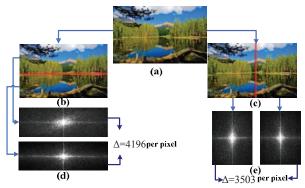

Figure 4. An example of features from Fourier domain. (b) and (d) show the Fourier transform with real reflection axis. (c) and (e) show the Fourier transform with fake reflection axis.

For local approach of reflection symmetry detection, SIFT descriptor is the most representative feature. As shown in Figure 5 (a), the desired result is that the SIFT saliency points are pairwised between the object and its reflection. Figure 5 (b) shows the real SIFT points detection and matching result using algorithm in [18]. Obviously, it is difficult to recognize the water reflection by matching the SIFT points.
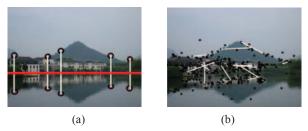

Figure 5. An example of SIFT saliency points detection and matching. (a) is the desired result, (b) is the real result of SIFT descriptor detection and matching.

3.2 Feature Distortion Caused by Motion Blur

Water reflection causes existing reflection symmetry detection techniques invalid mainly because the motion blur from water wave is large enough to distort the image features. Motion blur is a well known degradation factor due to the relative motion of the sensor and the scene in finite exposure time [23]. The formation model for the motion blur is:

$$g(x,y) = I(x,y) \otimes h(x,y) + n(x,y) \qquad (1)$$

where $I(x,y)$ is the original image, $h(x,y)$ is the point spread function (psf), $n(x,y)$ is additive noise and $g(x,y)$ is represents the observed image. Assume the linear translation motion function $Tm(t) = [Tm_x(t), Tm_y(t)]$ is known, $h(x,y)$ has the following form (2), where the Dirac delta function describes the two-dimensional displacement function of the image during the exposure interval $(t_o, t_o + t_e)$, t_e denotes the exposure period, and $1/t_e$ is a normalizing factor.

$$h(x,y) = \frac{1}{t_e} \int_{t_o}^{t_o + t_e} \delta[x - Tm_x(t), y - Tm_y(t)]dt \qquad (2)$$

Our eyes respond similar to a shutter speed of 1/30 second and the conventional cameras expose pictures 25 or 30 times per second [24]. Although the fastest shutter speed available is much higher now, 1/30 second is still commonly selected in landscape photography. The average phase velocity of water is about 0.3m/sec. So in every expose, one particle of the water will shift about 10mm in average. In the camera, the object distance u, image distance v and focal length f obey the Equation (3).

$$\frac{1}{u} + \frac{1}{v} = \frac{1}{f} \qquad (3)$$

Because in reality, $u \gg f$, it is reasonable approximate that the $v = f$. Based on this approximation, the angle of field 2ω, which describes the angular extent of a given scene that is imaged by a camera, has two relationships with the object and the image described in (4) and (5). x_r is the radius of field, and $2d$ is the size of the film (or sensor). Then we could get the Equation (6).

$$d = f \cdot tg\omega \qquad (4)$$

$$tg\omega = \frac{x_r}{u} \qquad (5)$$

$$\frac{u}{f} = \frac{x_r}{d} = \frac{\Delta x_r}{\Delta d} \qquad (6)$$

The motion in image could be denoted as $\Delta d = \Delta x \times (f/u)$. The focal length of human eyes to see the nature view is about 50mm, and we assume the object distance is 20000mm. As an example of 1/4 CCD, if the size of image is 640×480 pixels (30M), the pixel size $= 5 \times 5$ um. As a result, the motion $\Delta d \approx 10 \times (50/20000) \times (1/0.005) = 5$ pixels, i.e., the point in the object moves the distance about 5 pixels in the reflection part.

A conventional way to carry out motion blur object recognition is first to deblur the image, and then to apply the recognition methods. The core idea in deconvolution is to calculate the point spread function. For calculating the point spread function, we need to assume the velocity and direction of motion blur is unique [25] [26]. But water in nature is composed of a great quantity of waves with different frequency. And the velocity of different position in the wave profile with different frequency is various. It is impossible to remove the motion blur by calculating the point spread function even we simplify the water wave problem into a boundary value problem based on [27].

3.3 Motion Blur Invariance Space

The approach using invariant features appears to be the most promising and has been used extensively due to its relative low computation complexity and easily representation. The basic idea of invariant features is to describe the objects by a set of measurable quantities called invariants that are insensitive to particular deformations and could distinguish objects belonging to different classes. From a mathematical point of view, invariant Iv is a functional defined that does not change its value under degradation operator De, i.e. that satisfies the condition $Iv(I) = Iv(De(I))$ for any image function I. In practice, in order to accommodate the influence of imperfect segmentation, intra-class variability and noise, we usually formulate this requirement as a weaker constraint: $Iv(I)$ should not be significantly different from $Iv(De(I))$, just as $|Iv(I) - Iv(De(I))| < \varepsilon_{threshold}$.

As we described above, the key to address the problem resulted from the motion blur of water wave is to find invariants features. The history of moment invariants began in the nineteenth century under the framework of group theory and the theory of algebraic invariants. Moment invariants were first introduced to the pattern recognition and image processing community in 1962 [28]. Since that time, the research of moment invariants obtained deep improvements, extensions and generalizations and used in many areas of application. There have been numerous papers on moment invariants to affine and projective transforms, to photometric changes and to linear filtering of an image [29][30].

Image moments are weighted averages (moments) of the image pixels' intensities, or functions of those moments, usually chosen to have some attractive property. Compared with color histogram, the shift of moment due to the change of illumination is minimal [31] which often happens in water part.

General moment M_{pq} of an image $I(x, y)$ is defined as:

$$M_{pq} = \iint_D p_{pq}(x, y) I(x, y) dx dy \qquad (7)$$

where p, q are non-negative integers and $r = p + q$ is called the order of the moment, and $p_{00}(x, y), p_{10}(x, y), ..., p_{kj}(x, y), ...$ are polynomial basis functions. The most common choice is a standard power basis $p_{kj}(x, y) = x^k y^j$ that leads to geometric moments:

$$m_{pq} = \int_{-\infty}^{\infty} \int_{-\infty}^{\infty} x^p y^q I(x, y) dx dy \qquad (8)$$

The central moments are defined as:

$$\mu_{pq} = \int_{-\infty}^{\infty} \int_{-\infty}^{\infty} (x - \bar{x})^p (y - \bar{y})^q I(x, y) dx dy \qquad (9)$$

where $\bar{x} = m_{10} / m_{00}$ and $\bar{y} = m_{01} / m_{00}$ are the components of the centroid. If $I(x, y)$ is a digital image, Equation (8) and (9) are changed into (10) and (11).

$$m_{pq} = \sum_x \sum_y x^p y^q (x, y) \qquad (10)$$

$$\mu_{pq} = \sum_x \sum_y (x - \bar{x})^p (y - \bar{y})^q I(x, y) \qquad (11)$$

Moments η_{pq} where $p + q \geq 2$ can be constructed to be invariant to both translation and changes in scale by dividing the corresponding central moment by the properly scaled (00) th moment, using the following formula.

$$\eta_{pq} = \frac{\mu_{pq}}{\mu_{00}^{(1 + \frac{p+q}{2})}} \qquad (12)$$

When we neglect the additive noise $n(x, y)$, the observed image $g(x, y)$ in (1) could be denoted as (13).

$$g(x, y) = I(x, y) \otimes h(x, y) \qquad (13)$$

In motion blur case, the $(p + q)$ th geometric moments of the original image is defined as $m_{pq}^{(I)}$, the $(p + q)$ th geometric moments of the blurred image is defined as $m_{pq}^{(g)}$, the $(p + q)$ th central moments of the original image is defined as $\mu_{pq}^{(I)}$, and the $(p + q)$ th central moments of the blurred image is defined as $\mu_{pq}^{(g)}$.

According to the properties of Dirac delta function, $\mu_{pq}^{(h)} = 0$ for every $q \neq 0$, and if $(p + q)$ is odd, then $\mu_{pq}^{(h)} = 0$. Geometric moments of the blurred image $m_{pq}^{(g)}$ and Geometric moments of the original image $m_{pq}^{(I)}$ could be proved has the relationship (14). In similarly, $\mu_{pq}^{(g)}$ and $\mu_{pq}^{(I)}$ has the relationship (15).

$$m_{pq}^{(g)} = \sum_{k=0}^p \sum_{j=0}^q C_p^k \times C_q^j \times m_{kj}^{(f)} \times m_{kj}^{(h)} \qquad (14)$$

$$\mu_{pq}^{(g)} = \sum_{k=0}^p \sum_{j=0}^q C_p^k \times C_q^j \times \mu_{kj}^{(h)} \times \mu_{p-k,q-j}^{(I)} \qquad (15)$$

Derived from Hu's moment invariants [28], we construct the motion blur invariance space (MBIS) which is composed of four motion blur invariant moments in (16).

$$\begin{cases} IR_{m_1} = (\eta_{30} - 3\eta_{12})^2 + (3\eta_{21} - \eta_{03})^2 \\ IR_{m_2} = (\eta_{30} + \eta_{12})^2 + (\eta_{21} + \eta_{03})^2 \\ IR_{m_3} = (\eta_{30} - 3\eta_{12})(\eta_{30} + \eta_{12})[(\eta_{30} + \eta_{12})^2 - 3(\eta_{21} + \eta_{03})^2] \\ \quad + (3\eta_{21} - \eta_{03})(\eta_{21} + \eta_{03})[3(\eta_{30} + \eta_{12})^2 - (\eta_{21} + \eta_{03})^2] \\ IR_{m_4} = (3\eta_{21} - \eta_{03})(\eta_{30} + \eta_{12})[(\eta_{30} + \eta_{12})^2 - 3(\eta_{21} + \eta_{03})^2] \\ \quad + (\eta_{30} - 3\eta_{12})(\eta_{21} + \eta_{03})[3(\eta_{30} + \eta_{12})^2 - (\eta_{21} + \eta_{03})^2] \end{cases} \qquad (16)$$

4. Reflection Cost Minimization

In this section, we formulate water reflection recognition to an optimization problem and propose an efficient algorithm called reflection cost minimization (RC M) using DP.

4.1 Water reflection formulation

Because water reflection is imperfect reflection symmetry, the definition of reflection symmetry is given firstly.

Definition 1 A set $S \in R^n$ is reflection symmetric with respect to the vector (reflection axis) $<\cos\alpha_0, \sin\alpha_0>$ based on a reflection transform T_{D_K}, if $\forall x_i \in S, \exists x_j \in S$, s.t,

$$x_j = T_{D_K} x_i \tag{17}$$

where for $x_i \in \mathbb{R}^2$, T_{D_K} is given by

$$T_{D_K}(x,y) = \begin{pmatrix} \cos 2\alpha_0 & \sin 2\alpha_0 & 0 \\ \sin 2\alpha_0 & -\cos 2\alpha_0 & 0 \\ 0 & 0 & 1 \end{pmatrix}\begin{pmatrix} x \\ y \\ 1 \end{pmatrix} \tag{18}$$

So an image $I(x), \forall x \in \mathbb{R}^2, x = \begin{bmatrix} x \\ y \end{bmatrix}$, if it is said to have the reflection symmetry with the reflection axis $<\cos\alpha_0, \sin\alpha_0>$, obeys the Equation (19).

$$I(x) = I(T_{D_K}(x)), \forall x \in \mathbb{R}^2 \tag{19}$$

Because water reflection is imperfect reflection symmetry, in most of conditions, (19) could not be strictly complied with in imperfect symmetry due to the complexity of the water part in image with water reflection. It means that in water reflection case, the difference between $I(x)$ and $I(T_{D_K}(x))$ is not equal to zero.

Based on the analysis, we transform the water reflection problem into an optimization problem based on the complex moment invariants feature descriptors given by (20). In (20), IR_{thresh} is the threshold to distinguish water reflection with no water reflection, α_0^* is the tilt angle of the reflection axis.

$$\begin{cases} \alpha_0^* = \arg\min | \sum_{i=1}^{4} IR_{m_i}(I(x)) - \sum_{i=1}^{4} IR_{m_i}(I(T_{D_K}(x))) | \\ \min | \sum_{i=1}^{4} IR_{m_i}(I(x)) - \sum_{i=1}^{4} IR_{m_i}(I(T_{D_K}(x))) | \le IR_{thresh} \end{cases} \tag{20}$$

In order to detect the possible reflection axis, we could find the global optimization axis by exhaust algorithm, but it requires excessive computation even for small images.

To avoid excessive computation, we firstly do some simplifications to the optimization function. Then an efficient search algorithm is proposed to solve the optimization problem based on DP. Later, we compare the difference of computational complexity between exhaust algorithm and our algorithm.

In nature, water reflection often does not happen in the whole image and the reflection axis is often not complete or straight. Taking these situations into consideration, we do some simplifications based on the optimized problem shown in (20). Firstly, images are separated into M_s sub-images vertical to the supposed reflection axis direction DI_{α_0}. To every sub-image $I_j, 1 \le j \le M_s$, candidate reflection axis is denoted as $RA_{j,l}, 1 \le j \le M_s, 1 \le l \le H_{\alpha_0}$, where H_{α_0} is the height of the

sub-image I_k. The sum difference of moment invariants $DF_{j,k,l}$ of two sub-block $I_{j,k,l}^{up}(x)$ and the reversed sub-block $I_{j,k,l}^{rev\_down}(x)$ which located on both sides of line $RA_{j,l}$ is denoted as (21), where k is the height of sub-block which is above T_k.

$$DF_{j,k,l} = \sum_{i=1}^{4}[IR_{m_i}(I_{j,k,l}^{up}(x)) - IR_{m_i}(I_{j,k,l}^{rev\_down}(x))] \tag{21}$$

Reflection axis distance $DS_{j,l}$ is utilized to measure the continuity of the adjacent reflection axis which is denoted as (22).

$$DS_{j,l} = \begin{cases} \|RA_{j,l} - RA_{j+1,l}\|/T_d + 1 & j \le M_s - 1 \\ 1 & j = M_s \end{cases} \tag{22}$$

In this equation, $\|RA_{j,l} - RA_{j+1,l}\|$ is to describe the vertical distance between the candidate reflection axis in adjacent sub-image I_j and I_{j+1}. T_d is the factor used to normalize the distance to an specified range.

Then, we define the reflection cost RC in the current slide window $SW_m, 1 \le m \le H_{\alpha_0} - W_{sw}$ which is decided by $DF_{j,k,l}$ and $DS_{j,l}$ in Equation (23). The slide window SW_m with width W_{sw} is horizontal to the candidate reflection axis direction. The location of the centerline in SW_m is denoted as L_m where $L_m = m + W_{sw}/2$. The minimum of the reflection cost RC in all slide windows is denoted as MIN_{RC}. And the optimized reflection axis which is composed of RA_{j,l^*} in every sub-image I_j of slide window SW_m^* with the minimum of the reflection cost is denoted as (24).

$$RC = \sum_{j=1}^{M_s}(DF_{j,k,l} \times DS_{j,l}), \tag{23}$$
$$T_k \le k \le \frac{H_{\alpha_0}}{2}, l \in SW_m, 1 \le m \le H_{\alpha_0} - W_{sw}, -\frac{\pi}{2} \le \alpha_0 \le \frac{\pi}{2}$$

$$[\alpha_0^*, SW_m^*, RA_{1,l^*}, RA_{2,l^*}, ... RA_{M_s,l^*}] = \arg\min[\sum_{j=1}^{M_s}(DF_{j,k,l} \times DS_{j,l})] \tag{24}$$

The goal of this optimization problem is to find MIN_{RC} and the optimized reflection axis in the image.

4.2 Reflection cost minimization via Dynamic programming

The optimization problem of RCM we described in (23) and (24) is quite like the problem which is often solved by dynamic programming (DP). DP is both a mathematical optimization method and a computer programming method. In both contexts it refers to simplifying a complicated problem by breaking it down into simpler sub-problems in a recursive manner. In addition, even we have these simplifications, and DP is utilized to find the minimum moment cost, this work is still very difficult. So we have a preprocessing work before DP to limit the number of candidate reflection axis $RA_{j,l}$ in every sub image I_j. We rank the differences of

moment invariants $DF_{j,k,l}$, and only those $RA_{j,l}$ whose difference is fallen into the M_n minimum value are considered as the candidate reflection axis.

Then we define some basic concepts and variables in DP for water reflection problem. The *Stage variable* $K = j, 1 \le j \le M_s$ is used to describe the current stage or sub-image. The *State variable* λ_K is to describe the state as every stage. In our algorithm $\lambda_K = RA_{j,l}$ is the candidate reflection axis in the sub-image I_k. The *Space of State variable* Λ_K is the set of all possible *State variables*. In our problem, it is the set of all possible candidate reflection axes $RA_{j,l}$ whose difference is fallen into the M_n minimum value in the sub-image I_j. The *decision variable* u_K is defined as the decision based on the current state. In our case, u_K is the choice of the candidate reflection axis $RA_{j+1,l}$ in the next sub image I_{j+1}. And the *Transition Function* is defined as $\lambda_{K+1} = u_K$. The *Object function* is defined as (25) where v_K is the minimum of reflection cost in stage K denoted in (26).

$$V = \sum_{K=1}^{M_s} v_K(\lambda_K, u_K) \tag{25}$$

$$v_K = \min[DF_{j,k,l} \times DS_{j,l}], K=j, T_k \le k \le \frac{H_{\alpha_0}}{2}, l \in SW_m, 1 \le m \le H_{\alpha_0} - W_{sw}, -\frac{\pi}{2} \le \alpha_0 \le \frac{\pi}{2} \tag{26}$$

Our DP function is denoted as (27), where $f_K(\lambda_K)$ is the minimum of the reflection cost in every stage K in current SW_m.

$$\begin{cases} f_K(\lambda_K) = \min\{v_K(\lambda_K, u_K) + f_{K-1}(\lambda_{K-1})\} \\ \lambda_K \in \Lambda_K \qquad K = j, 1 \le j \le M_s \\ \lambda_{K+1} = u_K \end{cases} \tag{27}$$

Then we solve the (27) by positive sequence method to get the optimized policy in current slide window SW_m. After it, we could get MIN_{RC} which is the minimum of all RC in different slide windows and in different α_0 which is calculated by Equation (28).

$$MIN_{RC} = \min(f_{MS}(\lambda_{M_s})), 1 \le m \le H_{\alpha_0} - W_{sw}, -\frac{\pi}{2} \le \alpha_0 \le \frac{\pi}{2} \tag{28}$$

4.3 Algorithm and complexity analysis

In this part, the algorithm about the calculation of MIN_{RC} is described.

Algorithm 2 Calculation the minimum moment cost

Input: Image $I(x), x \in \mathbb{R}^2$, **Number of sub-block** $M_s = 6$, **Height of the sub-image** H_{α_0}, **Height threshold of sub-block** $T_j = H_{\alpha_0}/5$, **Number of candidate reflection axis** $M_n = H_{\alpha_0}/4$ **Normalization factor** $T_d = H_{\alpha_0}/12$. **The width of slide window** W_{sw}.

Output: Minimum moment cost MIN_{RC}

1. Sum difference of moment invariants calculation by (21)

$$\text{for } \alpha_0 = -\frac{\pi}{2}, ..., \frac{\pi}{2} \text{ do}$$
$$\quad \text{for } j = 1, ..., M_s \text{ do}$$
$$\quad\quad \text{for } l = 1, ..., H_{\alpha_0} \text{ do}$$
$$\quad\quad\quad \text{for } k = T_k, ..., H_{\alpha_0}/2 \text{ do}$$
$$\quad\quad\quad\quad DF_{j,k,l} = \sum_{i=1}^{4}[IR_{m_i}(I_{j,k,l}^{up}(x)) - IR_{m_i}(I_{j,k,l}^{rev\_down}(x))]$$
$$\quad\quad\quad \text{end for}$$
$$\quad\quad \text{end for}$$
$$\quad \text{end for}$$
$$\text{end for}$$

2. Rank the differences of moment invariants $DF_{j,k,l}$ for every α_0, contain those $RA_{j,l}$ whose $DF_{j,k,l}$ value fallen into the M_n minimum as the candidate reflection axis.

3. Reflection axis distance $DS_{j,l}$ calculated by (22)

$$DS_{j,l} = \begin{cases} \|RA_{j,l} - RA_{j+1,l}\| / T_d + 1 & j \le M_s - 1 \\ 1 & j = M_s \end{cases}$$

4. Minimum moment cost in stage K calculated by (26)

$$v_K = \min[DF_{j,k,l} \times DS_{j,l}], K=j, T_k \le k \le \frac{H_{\alpha_0}}{2}, l \in SW_m, 1 \le m \le H_{\alpha_0} - W_{sw}, -\frac{\pi}{2} \le \alpha_0 \le \frac{\pi}{2}$$

5. Minimum moment cost calculation by DP function step by step for every α_0 by (27)

$$\begin{cases} f_K(\lambda_K) = \min\{v_K(\lambda_K, u_K) + f_{K-1}(\lambda_{K-1})\} \\ \lambda_K \in \Lambda_K \qquad K = j, 1 \le j \le M_s \\ \lambda_{K+1} = u_K \end{cases}$$

6. Minimum moment cost MIN_{RC} calculated (28)

$$MIN_{RC} = \min(f_{MS}(\lambda_{M_s})), 1 \le m \le H_{\alpha_0} - W_{sw}, -\frac{\pi}{2} \le \alpha_0 \le \frac{\pi}{2}$$

Now, we will compare the difference of computational complexity between exhaust algorithm and our proposed RCM algorithm. For simplicity, we only calculate that the computational complexity to find the optimization axis in direction α_0. To every image, if we utilize the exhaust algorithm to find the global optimization axis, the complexity is $O((W_{sw}^{M_s} + W_{sw}^{M_s} \times \log_2(W_{sw}^{M_s})) \times H_{\alpha_0})$. If the proposed dynamic programming algorithm is utilized, the complexity is $O((M_s - 1) \times W_{sw}^2 \times \log_2(W_{sw})^2 \times H_{\alpha_0})$. It is obvious that the computational complexity of our algorithm is much lower than that of exhaust algorithm.

5. EXPERIMENT AND DISCUSSION

To demonstrate performance of our proposed technique, we conduct three experiments, including classification of the images with and without water reflection, detection of axis of reflection, and retrieval of the images with water reflection. For the proposed techniques, the parameter M_s, T_k, T_d and M_n, actually shows stable performance under different values. In our experiments, we

set $M_s = 6$, $T_k = H_{\alpha_0} / 5$, $T_d = H_{\alpha_0} / 12$, $M_n = H_{\alpha_0} / 4$, $W_{sw} = H_{\alpha_0} / 25$.

5.1 Classification Experiment

In the first experiment, for evaluating the classification accuracy of proposed technique, we construct the dataset including 50 images with water reflection and 50 nature scene images without water reflection. Figure 6 shows thumbnails of the images with water reflection and without water reflection used in the first experiment.

Figure 6. Example images in classification experiment. The first row shows the images with water reflection and the second row shows the images without water reflection.

We subdivide this dataset equally into five folders, and conduct fivefold cross validations for the learning algorithms. Every time, we utilize one folder for testing, and the other four folders for training. If MIN_{RC} is below the threshold IR_{thresh} learnt by binary SVM based on the training dataset, this image is classified as the image with water reflection. The classification accuracy results are shown in Table 1. "Classification accuracy" is abbreviated by Ca, "Water reflection" is abbreviated by W_r. The performance shows that our proposed technique based on MBIS could be effectively distinguish the water reflection images with non water reflection images.

Table 1. Classification accuracy

Trail	1	2	3	4	5
Ca of W_r	90%	80%	90%	90%	80%
Ca of non W_r	80%	80%	80%	90%	80%
Ca of all	85%	80%	85%	90%	80%

5.2 Detection the Reflection Axis Experiment

To compare with existing symmetry algorithms, the detection experiment on 100 images with water reflection is carried out. The goal of our experiment is to detection the reflection axis. We compare with the representative algorithm of Loy *et al.* [18], who chose SIFT detection points as interesting salient points and took advantage of pairwise matching of their SIFT descriptors to detect axis of symmetry. The accuracy of axis detection of their algorithm is 29%, and the accuracy of axis detection of our algorithm is 84%. In Figure 7, we give some examples to illustrate the detection results. Our detection results are shown in first and third row. And results of [18] are shown in the second and fourth row. It is obvious that our algorithm is more effective than theirs.
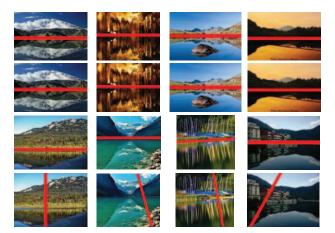

Figure 7. Performance comparison of reflection axis detection. Our detection results are shown in first and third row. And results of [18] are shown in the second and fourth row.

5.3 Retrieval Experiment

For evaluating the performance of the proposed technique, we apply it in text based image retrieval. The textual query is "water reflection", every image which is related to this concept is returned. The dataset downloaded from Google contains two parts, the first part is 50 images with water reflection and the second part is 10000 images without water reflection. Figure 8 shows thumbnails of the images with and without water reflection used in the retrieval experiment.

Figure 8. Example images with and without water reflection in retrieval experiment.

In our experiment, we use four popular evaluation measures of evaluating the performance of image retrieval systems, precision, recall, Average precision and NDCG. The Precision and Recall results of retrieval experiment are shown in Table 2. The number of retrieval sample is from 10 to 50 with increments of 10. Precision and recall are single-value metrics based on the whole list of documents returned by the retrieval system. For systems that return a ranked sequence of images, it is desirable to also consider the order in which the returned images are presented. So we also present the results of AveP and NDCG in Figure 9.

Table 2. Precision and recall results of retrieval experiment

Retrieval Number	10	20	30	40	50
Precision	70%	70%	73%	73%	72%
Recall	14%	28%	44%	58%	72%

5.4 Discussion

According to three experiments and different kinds of evaluation, our motion blur invariance space and algorithms are effective in water reflection detection and recognition. Figure 10 shows the thumbnails of first eight images without water reflection but these images are finally retrieved out. It is easily to find that these images are imperfect symmetry. We are sure it is the limitation of our algorithm, that our algorithm cannot distinguish the image with water reflection with the imperfect symmetry image. In future, we will focus on how to distinguish images with water reflection from other imperfect symmetry images.

6. CONCLUSION

In this paper, to address the difficulty in water reflection recognition, we construct a set of features in motion blur invariance space (MBIS). Moreover, we propose an efficient water reflection classification and axis detection algorithm RCM using dynamic programming. The experiments on three real image datasets have demonstrated impressive results of the proposed feature space and techniques.
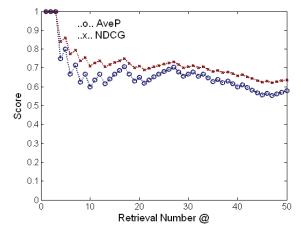

Figure 9. AveP and NDCG results of the retrieval experiment.

Figure 10. Experiment images that the proposed algorithm wrongly retrieve as the water reflection.

7. REFERENCES

[1] Nasar, J.L. & Li, M., "Landscape mirror: the attractiveness of reflecting water, "*Landscape and Urban Planning*, vol(66), pp.233-238, 2004.

[2] P. Felzenszwalb and D. Huttenlocher, "Efficient graph-based image-segmentation", In *IJCV*, 59(2), pp.167–181, 2004.

[3] Hua Zhang, Xiaojie Guo, Xiaochun Cao, "Water reflection detection using a flip invariant shape detector", In *ICPR*, pp. 633-636, 2010.

[4] S. Lee, R.Collins, Y. Liu, "Rotation symmetry group detection via frequency analysis of frieze-expansions", In *CVPR.*, June 2008.

[5] T. Kanade and J. R. Kender. "Mapping image properties into shape constraints: skewed symmetry, affine-transformable patterns, and the shape-from-texture paradigm," In *Human and Machine Vision,* pp. 237–257. Academic Press, 1983.

[6] D. Shen, H.H.S. Ip, and E.K. Teoh., "Robust detection of skewed symmetries", In *ICPR*, vol.3, pp. 1010–1013, 2000.

[7] Y. Lei and K. C. Wong, "Detection and Localisation of Reflectional and Rotational Symmetry under Weak Perspective Projection", *Pattern Recognition*, vol. 32, pp. 167-180, 1999.

[8] H. Cornelius and G. Loy, "Detecting bilateral symmetry in perspective," In *ICPR*, 2006.

[9] H. Weyl. "Symmetry," *Princeton University Press*, 1952.

[10] S. Mitra and Y. Liu, "Local facial asymmetry for expression classification", In *CVPR*, pp. 889 – 894, June 2004.

[11] A. Kuehnle., "Symmetry-based recognition of vehicle rears," In *PR*, vol. 12(4), pp. 249–258, 1991.

[12] M. Mancas, B. Gosselin, and B. Macq "Fast and automatic tumoral area localisation using symmetry," In *ICASSP*, pp.725–728, 2005.

[13] J. Podolak, A. Golovinskiy, and S. Rusinkiewicz, "Symmetry-enhanced remeshing of surfaces", In *Symposium on Geometry Processing*, July 2007.

[14] A.D. Gross, T.E. Boult, "Analyzing skewed symmetries" ,In *Int. J. Comput. Vision*, vol.13, pp.91-111, 1994.

[15] L. Lucchese, "Frequency domain classification of cyclic and dihedral symmetries of finite 2-D Patterns," In *PR*, 37:2263–2280, 2004.

[16] S. Derrode and F. Ghorbel, "Shape analysis and symmetry detection in gray-level objects using the analytical Fourier-Mellin representation," In *Signal Processing*, 84(1), pp. 25–39, 2004.

[17] S.A. Friedberg, "Finding axes of skewed symmetry", In *Comput. Vision Graphics Image Process*, vol.34, pp.138-155, 1986.

[18] G. Loy and J. Eklundh, "Detecting symmetry and symmetridc constellations of features," In *ECCV*, pp. 508-521, May 2006.

[19] L. van Gool, T. Moons, D. Ungureanu, E. Pauwels, "Symmetry from shape and shape from symmetry", In *Int. J. Robotics Res*, vol.14 (5), pp.407-424, 1995.

[20] L. van Gool, T. Moons, D. Ungureanu, A. Oosterlinck, "The characterisation and detection of skewed symmetry", In *Comput. Vision Image Understanding*, vol.61 (1), pp.138-150, 1995.

[21] T.J. Cham, R. Cipolla, "Symmetry detection through local skewed symmetries",In *Image Vision Comput,* vol.13 (5) , pp.439-450, 1995.

[22] K.S.Y. Yuen, W.W. Chan, "Two methods for detecting symmetries", In *Patt. Rec. Lett*. vol.15 (3) , pp.279-286, 1994.

[23] J. Flusser, T. Suk and S. Saic, "Recognition of images degraded by linear motion blur without restoration," *Computing Suppl.,* vol. 11, pp. 37-51, 1996.

[24] http://en.wikipedia.org/wiki/Motion_blur

[25] X.Y.Qi, L.Zhang, C.L. Tan, "Motion deblurring for optical character recognition," In *ICDAR*, pp. 389-393, 2005.

[26] J. H., C.Q. Liu, C. "Motion blur identification from image gradients," In *CVPR*, pp. 1-8, 2008.

[27] J. N. Newman, "Marine Hydrodynamics", *MIT Press*, 1977.

[28] Hu, M.-K. "Visual pattern recognition by moment invariants," *IRE Transactions on Information Theory*, vol. 8(2), 1962.

[29] J. Flusser, "Moment invariants in Image Analysis," In *Proceedings of World Academy of Science, Engineering and Technology.,* vol. 11, 2006.

[30] J. Flusser, "Moment forms invariant to rotation and blur in arbitrary number of dimensions," In *PAMI.,* vol. 25(2), pp. 234-246, 2003.

[31] M. K. Mandal, T. Aboulnasr, and S. Panchanathan, "Image indexing using moments and wavelets", *IEEE Trans. Consumer Electron.*, vol. 42, pp. 557 - 565, 1996.